ACS Catalysis

pubs.acs.org/acscatalysis Research Article

Engineering *Escherichia coli* Pyruvate Metabolism to Generate Noncanonical Reducing Power

Derek Aspacio,[#] Emma Luu,[#] Suphanida Worakaensai,[#] Youtian Cui, Sarah Maxel, Edward King, Raine Hagerty, Alexander Chu, Derek Minn, Justin B. Siegel, and Han Li*

Cite This: *ACS Catal.* 2024, 14, 9776–9784 Read Online

ACCESS | Metrics & More | Article Recommendations | Supporting Information

ABSTRACT: The future of biomanufacturing is dependent on rewiring biological systems to establish an alternative approach to our current chemical industries. However, a key limitation in biomanufacturing is that desired processes must rely on the same two redox cofactors as natural metabolism, nicotinamide adenine dinucleotide (phosphate) NAD(P)$^+$, to shuttle electrons energy. Thus, competition of resources with natural reactions within host cells is nearly unavoidable. One strategy to overcome redox cofactor resource competition is the implementation of a third, noncanonical redox cofactor, such as nicotinamide mononucleotide (NMN$^+$), which supports specific electron delivery to desired reactions. Here, we redesign the *Escherichia coli* pyruvate dehydrogenase multienzyme complex (PDHc) to specially utilize NMN$^+$ by engineering its E3 subunit (Lpd). Through rational design, we discover a cofactor promiscuous variant Lpd Penta (G182R-I186T-M206E-E205W-I271L) with an ∼2500-fold improvement in NMN$^+$ apparent turnover number. We tailor the enzyme to exclusively use NMN$^+$ through computational design and construct Lpd Ortho (Penta-R292E-Q317L) with a 2.4 × 10^5-fold cofactor specificity improvement toward NMN$^+$ compared to the wild type. Molecular simulation allowed tracking of the cofactor's alternative binding poses that emerge as the enzyme evolves, which was crucial to precisely guide engineering. We demonstrate that the engineered NMN$^+$-specific PDHc functions in *E. coli* cells to sustain the life-essential pyruvate metabolism, in an NMN$^+$-dependent manner. These results expand the available NMN$^+$ toolkit to include the high flux and nearly irreversible reaction of PDHc as an insulated electron source.

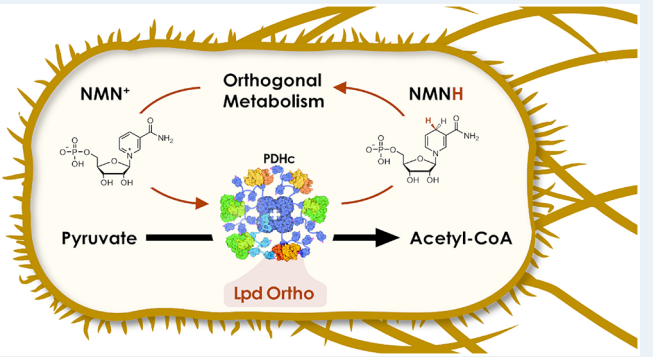

KEYWORDS: *pyruvate dehydrogenase complex, nicotinamide mononucleotide, noncanonical redox cofactor, rational protein design, orthogonal pathway engineering, dihydrolipoamide dehydrogenase, biomimetic cofactor*

INTRODUCTION

Biomanufacturing applies biological systems toward large-scale synthesis of commodity and specialty chemicals, presenting an alternative means of sustainable production that does not rely upon fossil fuel-based carbon. Biomanufacturing approaches have been classified as two primary thrusts that focus on whole-cell fermentation[1−3] or cell-free biotransformation.[4−6] However, systems within both biomanufacturing thrusts often depend entirely upon cofactors such as nicotinamide adenine dinucleotide (NAD(H)) and nicotinamide adenine dinucleotide phosphate (NADP(H)) to shuttle electron energy.

However, these natural redox cofactors are shared by the myriad competing reactions within host cells, which prohibits directing their reducing power exclusively to a desired biotransformation; this leads to side product formation. For fermentations, where biocatalyst is autocatalytically regenerated at low cost by cellular reproduction, resolving this critical issue requires *tour-de-force* genetic knockout campaigns to address.[7−9] Alternatively, in vitro biotransformation can resolve the issue of competing pathways by isolating the time and space in which reactions occur;[4,5] however, complete reaction isolation requires costly biocatalyst purification to near homogeneity; this exacerbates a major challenge in synthetic biochemistry, the presently high costs of input enzyme production.[10,11]

One strategy to overcome redox cofactor resource competition with native reactions is the implementation of a third, noncanonical redox cofactor. Such a cofactor must possess the structural deviation necessary to avoid recognition by natural enzymes and preserve the structural conservation of the redox-active functionality. We and others have established

Received: April 10, 2024
Revised: May 31, 2024
Accepted: June 5, 2024
Published: June 14, 2024

https://doi.org/10.1021/acscatal.4c02131
ACS Catal. 2024, 14, 9776−9784

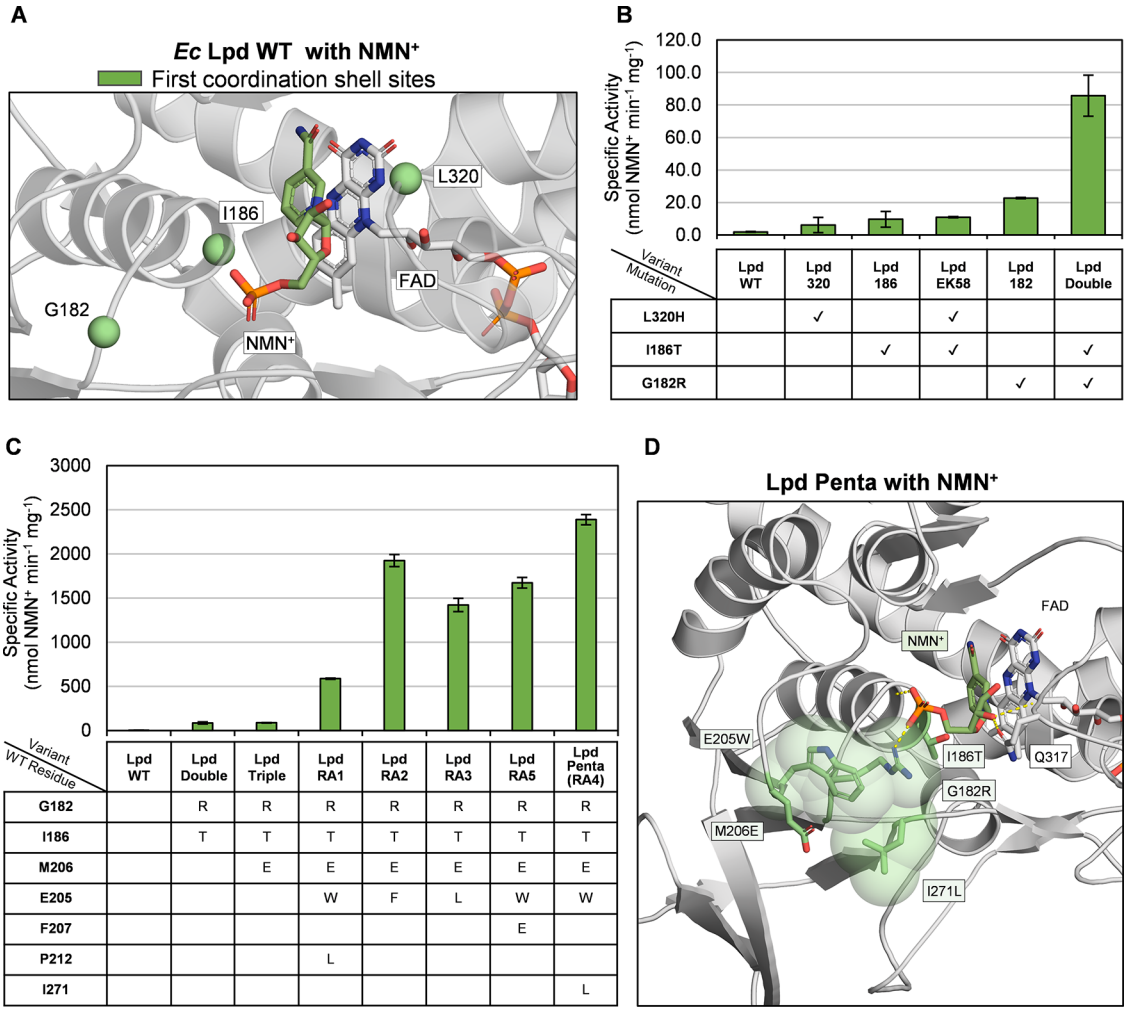

Figure 1. Engineering *Ec* Lpd to efficiently accept NMN^+ as a cofactor. (A) Sites chosen that could directly form polar contact to NMN^+ in a hypothetical, catalytically competent pose. (B) Specific activity of variants after the first rounds of NMN^+ engineering. Bars are the averages of duplicates. Error bars are one standard deviation. (C) Specific activity of variants constructed based on the premise of hydrophobic packing observed in *Lp* Nox. Bars represent the average of triplicates with an error of one standard deviation. (D) Model of Lpd Penta (G182R-I186T-M206E-E205W-I271L) with NMN^+ docked in the active site. Mutations G182R and I186T are expected to form polar interactions with phosphate on NMN^+. E205W and I271L are predicted to hydrophobically pack and hold G182R competent-binding position. M206E is predicted to reinforce the loop bearing E205W. Packing of mutations is visually emphasized by transparent spheres of approximate atomic van der Waals radii.

examples of noncanonical redox cofactors and have highlighted their advantages in comparison to natural systems, such as faster mass transport,[12] lower cost,[6,13−15] increased stability,[14,16,17] and support for specific electron delivery and retrieval.[15,18−25] Specific electron delivery and retrieval obviate the need to disrupt competing redox reactions in fermentation and decrease the degree of biocatalyst purification—thereby input enzyme cost—required to achieve high yield electron transfers in multienzyme cell-free systems. Thus, for biological systems, the understanding of the design rules for precise catalysts that interface high energy cofactors only as intended is broadly motivated by the present obstacles to deploying biocatalysts at scale.

Toward this end, we focus our efforts in this report on understanding the redox catalysis of the pyruvate dehydrogenase complex (PDHc) and how combinations of mutations affect its ability to interface NMN^+, NAD^+, and $NADP^+$. Previous reports of noncanonical reducing power generation have succeeded in storing reducing equivalents stemming from glycolytic pathways.[18,19,26] However, the high flux and practically irreversible reaction of PDHc have not been targeted as a source of noncanonical reducing power.

In this work, we engineer the PDHc of *Escherichia coli* to reduce nicotinamide mononucleotide (NMN^+), a model orthogonal redox cofactor.[18−20,22,27−29] We achieved this goal by engineering the cofactor specificity of *E. coli* dihydrolipoyl dehydrogenase (*Ec* Lpd), the E3 subunit of PDHc. First, we developed a variant, Lpd Penta, which represents an ∼2500-fold increase in apparent turnover number for NMN^+ relative to wild type (WT). Next, we tailor the enzyme toward NMN^+ specificity through computational design to construct Lpd Ortho with a 2.4×10^5-fold cofactor specificity improvement toward NMN^+, based on catalytic efficiency, compared to WT. Lastly, we demonstrate Lpd Ortho's function in vivo as an integral part of the PDH complex in *E. coli*, where pyruvate conversion to acetyl-CoA (AcCoA) only progresses when NMN^+ is supplied. These results suggest that the engineered, NMN^+-dependent PDHc is artificially controllable and can be repurposed to generate NMNH reducing power.

https://doi.org/10.1021/acscatal.4c02131
ACS Catal. 2024, 14, 9776−9784

Table 1. Apparent Michaelis–Menten Kinetic Parameters of the *Lpd* Variants[a]

variant (mutations)	cofactor	k_{cat} (s^{-1})	K_m (mM)	k_{cat}/K_m (mM^{-1} s^{-1})
Lpd WT	NAD^+	150 ± 10	1.1 ± 0.1	130 ± 10
	$NADP^+$	n.d.	n.d.	(8.7 ± 0.4) × 10^{-5}
	NMN^+	(1.7 ± 0.1) × 10^{-3}	8.3 ± 0.3	(2.1 ± 0.1) × 10^{-4}
Lpd Penta (G182R-I186T-M206E-E205W–I271L)	NAD^+	21 ± 1	25 ± 3	0.87 ± 0.09
	$NADP^+$	5.2 ± 0.2	29.3 ± 0.5	0.18 ± 0.01
	NMN^+	4.2 ± 0.2	28 ± 1	0.15 ± 0.01
RA17 (G182R-I186T-M206E-E205W–I271L-R292E)	NAD^+	33 ± 2	37 ± 3	0.9 ± 0.1
	$NADP^+$	n.d.	n.d.	0.019 ± 0.001
	NMN^+	3.2 ± 0.1	19 ± 2	0.17 ± 0.02
PF28 (G182R-I186T-M206E-E205W–I271L-Q317L)	NAD^+	n.d.	n.d.	0.27 ± 0.02
	$NADP^+$	0.92 ± 0.03	30 ± 3	0.03 ± 0.01
	NMN^+	3.7 ± 0.1	33 ± 2	0.11 ± 0.01
Lpd Ortho (G182R-I186T-M206E-E205W–I271L-R292E-Q317L)	NAD^+	n.d.	n.d.	0.25 ± 0.01
	$NADP^+$	n.d.	n.d.	(5.5 ± 0.1) × 10^{-3}
	NMN^+	3.4 ± 0.1	34 ± 1	0.099 ± 0.002

[a]Reactions were performed with 100 mM potassium phosphate at pH 8, 1.5 mM EDTA, and varying cofactor concentrations at 37 °C. For parameters marked "n.d.", the enzyme could not be saturated within the range of cofactor concentrations tested (up to 60 mM). Therefore, the data were fit to a simplified form of the Michaelis–Menten equation under the assumption that $K_m \gg S$, where reaction rate is linearly proportional to cofactor concentration with slope V_{max}/K_m. Values represent the mean ± one standard deviation of three independent replicates. Error apparent in catalytic efficiency is calculated by propagation of error when the Michaelis–Menten equation could be fit.

RESULTS AND DISCUSSION

Remodeling the *Ec* Lpd Cofactor Binding Site for NMN^+ Activity. In the first round of rational design, we targeted sites that could directly form novel polar contacts with the phosphate or ribose moieties of NMN^+ for mutagenesis (Figure 1A). As previously discussed,[18,19,22,27,29] NMN^+ displays a single, negatively charged phosphate group where the adenine nucleotide is truncated. We conducted single-site mutation of the first shell residues to polar or positively charged side chains. Our initial design round tested multiple sites based on the existing crystal structure of *Ec* Lpd WT (PDB: 4JDR, Figure 1A) with the goal of observing patterned changes to NAD^+, $NADP^+$, or NMN^+ activities in response to different cofactor binding site perturbations. Small libraries of variants at each site were designed, and the numbers further filtered on heuristics of distance, angle, and physiochemical property of the side chain. In the initial round, priority of designs was given to candidates at different amino acid positions rather than different mutations at a given site. This led to the discovery of three single mutants, L320H, I186T, and G182R, with improved NMN^+ activity relative to WT (Figure 1B). Since we achieved multiple NMN^+ activity boosting variants in the initial round, we immediately proceeded to construct combinations of these variants and arrived at the double mutant Lpd Double (I186T-G182R) with an improved specific activity for NMN^+ of 86 ± 10 nmol NMN^+ min^{-1} mg^{-1} (Figure 1B). In Lpd Double, the hydroxyl of I186T is predicted to form a hydrogen bond, and the guanidinium of G182R engages in an attractive electrostatic interaction with the exposed phosphate of NMN^+. Other combinations of the mutations did not show additive benefits (data not shown).

While *Ec* Lpd WT is highly specific for NAD^+, Lpd Double gained $NADP^+$-dependent activity, which contradicts our goal of engineering an NMN^+ specific enzyme. This improved activity might be due to G182R's recruitment of the 2′-phosphate in $NADP^+$. To neutralize the local positive charges where G182R resides, we constructed Lpd Triple (I186T-G182R-M206E), which returns $NADP^+$ activity back to the low levels observed in the WT (Figure S1). We proceeded with Lpd Triple as the template for further designs.

To further tune cofactor specificity of Lpd, we drew from our previous work on engineering a structurally similar enzyme,*Lactobacillus pentosus*water-forming oxidase (*Lp* Nox)[29] (Figure S2). We introduced bulky residues at positions E205, F207, P212, and I271 of Lpd Triple to create steric clashes in the cleft that the adenine of NAD^+ binds within, resulting in Lpd variants RA1 through RA5 (Figure 1C). Surprisingly, these mutations did not block the $NAD(P)^+$ activity as observed in the homologous *Lp* Nox variant—as discussed in the next section on designing for specificity. Instead, many of the variants show substantially increased NMN^+, NAD^+, and $NADP^+$ activities with the most active variant, Lpd Penta (G182R-I186T-M206E-E205W-I271L), displaying specific activity levels of 2400, 6200, and 1600 nmol cofactor min^{-1} mg^{-1}, respectively (Figures 1C and S3). We characterized Lpd Penta further by determining its apparent Michaelis–Menten kinetic parameters compared to those of WT with all three cofactors. In Lpd Penta, the turnover number, k_{cat}, for NMN^+ increases ~2500-fold relative to WT from 0.0017 to 4.2 s^{-1} (Table 1). However, Michaelis constant, K_m, for NMN^+ stays relatively high at ~28 mM. Altogether, Lpd Penta exhibits a 1.1 × 10^5-fold switch in cofactor specificity from NAD^+ to NMN^+ relative to WT based on catalytic efficiency (k_{cat}/K_m).

To better understand how these designs boost NMN^+ activity, we modeled Lpd Penta with the Rosetta Molecular Modeling Suite to investigate the structural basis for its improvement.[30] Our models predict that the key interaction that promotes NMN^+ activity in Lpd Penta compared to that in Lpd Triple is the packing of the side chain of E205W against G182R, thus restricting the conformational entropy of the flexible G182R side chain (Figure 1D). This forces G182R to narrowly sample the productive rotamer, where it is hypothesized to position NMN^+ for catalysis, consistent with the improved k_{cat} (Table 1). This mode of indirect tuning of the polar contact to NMN^+ is consistent with our past

https://doi.org/10.1021/acscatal.4c02131
ACS Catal. 2024, 14, 9776–9784

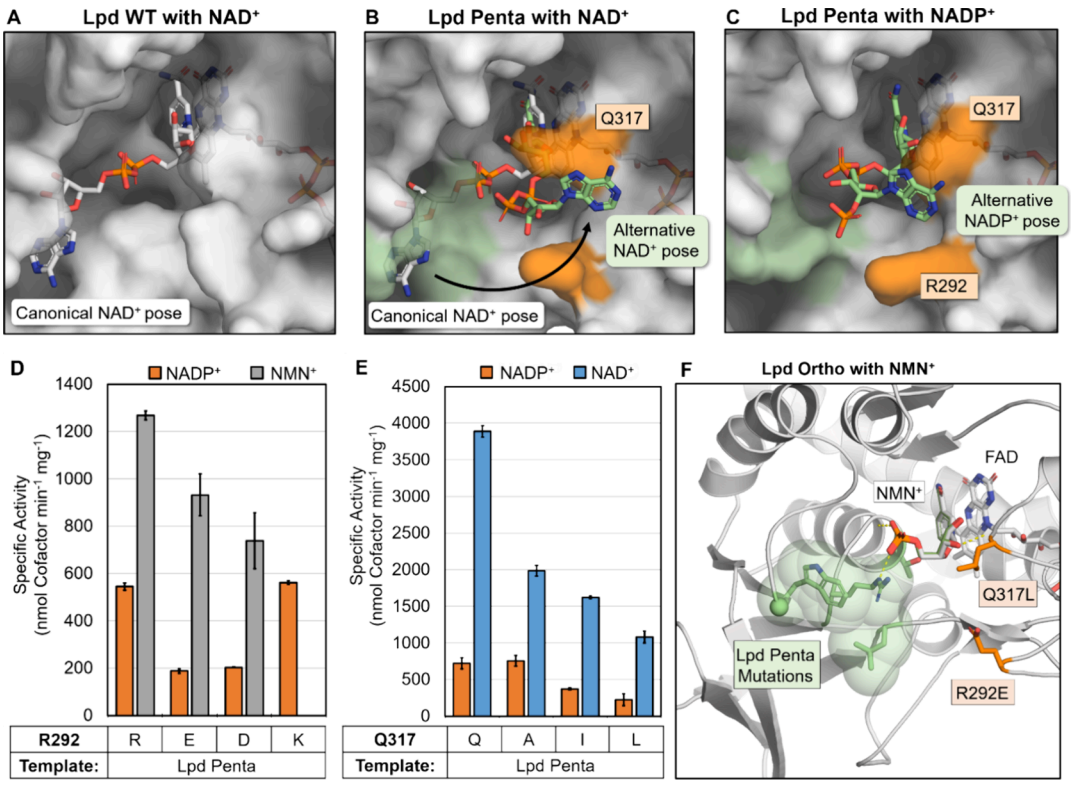

Figure 2. Engineering the cofactor specificity of Lpd Penta. (A) Model of the *Ec* Lpd WT NAD^+ binding pose based on NAD^+ bound crystal structures of related homologues. (B) Model of the predicted alternative NAD^+ binding pose in Lpd Penta. NAD^+ binding in Lpd Penta is predicted to swing from its native pose (white) within the Rossmann fold to an alternative site (green) due to the mutations that completely occlude the native cleft (green surface). Key residues for the alternative binding pose are colored as orange surface. (C) Model of the predicted alternative site for $NADP^+$ activity in Lpd Penta. Lpd WT has trace activity with $NADP^+$. (D) Specific activity of Lpd Penta R292 variants with 6 mM $NADP^+$ and 6 mM NMN^+. Variants with negatively charged side chains, E and D, decrease $NADP^+$ activity and retain NMN^+ activity. (E) Specific activity of Lpd Penta Q317 variants with 6 mM NAD^+ and 6 mM $NADP^+$. Different mutations at Q317 reveal the importance of polar contacts for remodeled NAD^+ and $NADP^+$ activities. Variants appear to rely on steric bulk to disrupt the activity. (F) Model of the predicted NMN^+ binding pose in Lpd Ortho compared to Lpd Penta. Lpd Ortho NMN^+ pose is shown in white. Overlay of aligned Lpd Penta NMN^+ binding pose is shown in green. Mutations unique to Lpd Ortho for blocking the alternative $NAD(P)^+$ binding poses are shown in orange. Mutations present in Lpd Penta are shown in green. Data represents the average of three replicates with error bars of one standard deviation.

computationally designed glucose dehydrogenase and glyceraldehyde-3-phosphate dehydrogenase variants.[18,19]

Serendipitously, the $NADP^+$ blocking mutation, M206E, with little effect on NMN^+ activity in Lpd Triple, was essential for the extreme cofactor binding site remodeling observed in Lpd Penta, and all activity was nearly abolished by its reversion to M206 (Figure S4A). In addition to low specific activity, lower soluble protein concentration was observed during its purification relative to Lpd Penta (Figure S4B). In our model of Lpd Penta, M206E is not predicted to make additional polar contacts and has no significant loop conformational changes relative to WT (Figure S4C,D). However, we speculate that M206E in Lpd Penta may prevent loop disruption after large changes to E205, since mutation E205W ablates the hydrogen bond network that holds the loop in place (Figure S4C,D).

Reactions were performed with 100 mM potassium phosphate at pH 8, 1.5 mM EDTA, and varying cofactor concentrations at 37 °C. For parameters marked "n.d.", the enzyme could not be saturated within the range of cofactor concentrations tested (up to 60 mM). Therefore, the data were fit to a simplified form of the Michaelis–Menten equation under the assumption that $K_m \gg S$, where reaction rate is linearly proportional to cofactor concentration with slope V_{max}/K_m. Values represent the mean ± one standard deviation of three independent replicates. Error apparent in catalytic efficiency is calculated by propagation of error when the Michaelis–Menten equation could be fit.

Computationally Guided Design of an Orthogonal *Ec* Lpd. Our most active variant, Lpd Penta, has high activity for NMN^+; however, its residual NAD^+ and $NADP^+$ activity (Table 1) prevents application in vivo where specific electron transfer to NMN^+ is desired. Therefore, we focused on designing mutations to specifically disrupt the $NAD(P)^+$ activity while retaining the NMN^+ activity. In the Lpd WT structure, NAD^+ binds within a conserved Rossmann fold motif (Figure 2A). Based on our models of Lpd Penta with $NAD(P)^+$, the restricted positioning of G182R causes the side chain to obstruct the binding pose for NAD^+ observed in homologous WT crystal structures (Figure 2B, pose colored white and obstructing surface colored green). Subsequent mutations naively designed to line the canonical $NAD(P)^+$ site in the crystal structure did not improve orthogonality (data not shown).

We hypothesized that the remaining $NAD(P)^+$ activity is a consequence of the remodeled binding site stabilizing alternative binding poses for the dinucleotide cofactors. Indeed, when we revisited high ranking alternative poses predicted in Rosetta, NAD^+ and $NADP^+$ are displaced from their canonical position at the Rossmann fold (Figure 2A) and

https://doi.org/10.1021/acscatal.4c02131
ACS Catal. 2024, 14, 9776−9784

instead are predicted to occupy an adjacent pocket (Figure 2B,C).

Our models predict that site Q317 directly contacts the alternative poses of NAD^+ and $NADP^+$ in Lpd Penta (Figure 2B,C). Therefore, we mutated Q317 to A, I, and L and discovered that variant PF28 (Lpd Penta Q317L) shows significant disruption of NAD^+ and $NADP^+$ activities (Figure 2E and Table 1). The catalytic efficiency for NAD^+ of PF28 decreases ~3-fold relative to that of Lpd Penta and ~6-fold for $NADP^+$ (Table 1). Rosetta models indicate that the Q317L mutation no longer sustains the $NAD(P)^+$ interaction through hydrogen bonding; it also sterically clashes with $NAD(P)^+$ without affecting NMN^+ (Figure 2F).

Site R292 is also predicted to be important in binding $NADP^+$; therefore, we introduced negatively charge (E and D) and positively charge (K) side chains to this position (Figure 2C,D). We discovered that variant RA17 (Lpd Penta R292E) decreases $NADP^+$ catalytic efficiency nearly 10-fold (Table 1) compared to Lpd Penta with small changes in apparent kinetic parameters for NAD^+ or NMN^+. R292 with its positive charges is hypothesized to electrostatically interact with the negatively charged 2' phosphate of $NADP^+$. Substitution R292E makes this position negatively charged instead.

Finally, we combined the mutations of variants RA17 and PF28 to produce variant Lpd Ortho (Lpd Penta R292E-Q317L). When compared to the predicted model for Lpd Penta, the mutations present in Lpd Ortho should not directly disrupt NMN^+ binding; indeed, high NMN^+ activity is maintained (Table 1 and Figure 2F; predicted poses for Lpd Penta and Lpd Ortho are shown in green and white, respectively). Altogether, when compared to WT, Lpd Ortho represents a 2.4×10^5-fold increase in cofactor preference based on catalytic efficiency from NAD^+, the native cofactor of PDHc, to NMN^+. Similar to the WT, Lpd Ortho features nominal $NADP^+$ activity and a very large K_m (beyond the 60 mM upper limit of cofactor concentrations tested) relative to the intracellular cofactor concentrations. In summary, Lpd Ortho is suitable for integration into PDHc which can then be used to generate the orthogonal reducing power, NMNH, specifically in vivo.

Orthogonal *Ec* Lpd Functions within Pyruvate Dehydrogenase Complex to Reduce NMN^+ In Vivo. We sought to determine whether our most orthogonal variant based on kinetic parameters could achieve two goals: (1) demonstrate that engineered Lpd variants could function within the context of the full PDHc and (2) demonstrate that Lpd Ortho could facilitate specific electron transfer to NMN^+ at physiological concentrations of $NAD(P)^+$. To assess both goals, we devised a strategy based on coupling cell growth to PDHc activity as a facile readout (Figure 3A). Our engineered strain SW3 (Δ*lpd* Δ*pncC* Δ*ushA*::tet Δ*pflB*) grows slowly on glucose because the genomic copy of *lpd* and pyruvate-formate lyase (encoded by *pflB*) are disrupted,[31,32] leading to inability to produce AcCoA. A detour exists through an oxygen-dependent cleavage of pyruvate to acetate, encoded by *poxB*, which, upon acetate activation could produce AcCoA. Although in the culture conditions tested, we observe the desired growth phenotype without further strain engineering to disrupt *poxB*. We complement the *lpd* knockout with *lpd* variants we engineered that are supplied on a plasmid. The strain also contains knockouts of NMN^+ degradation enzymes, *pncC*[33] and *ushA*.[34,35]

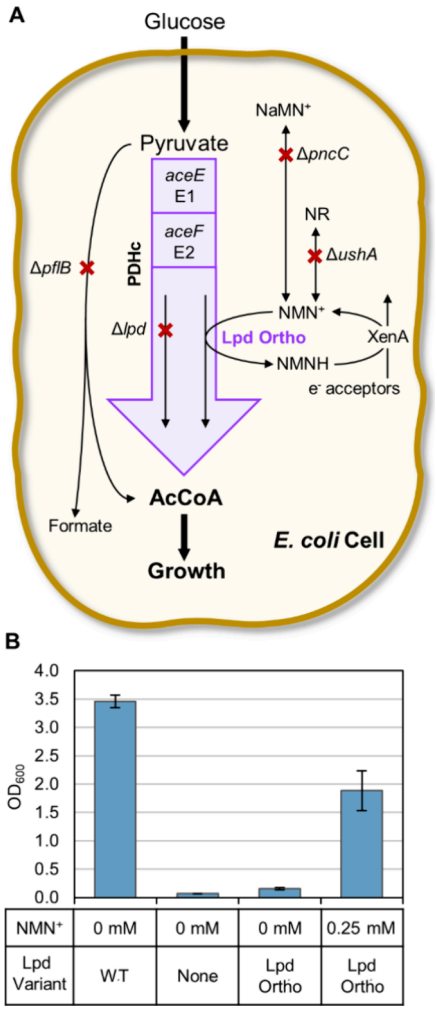

Figure 3. Lpd Ortho supports NMN^+-dependent growth of *E. coli*. (A) Engineered central carbon metabolism in strain SW3 (Δ*lpd* Δ*pncC* Δ*ushA*::tet Δ*pflB*) couples PDHc activity to growth on glucose because the strain cannot produce Acetyl-CoA (AcCoA) from glucose. NMN^+ is provided by supplementation to the growth medium. (B) Growth of AcCoA auxotroph strain after 19 h of culture at 30 °C. Growth study was initiated by addition of washed SW3 cells to 0.01 OD_{600} in M9 growth challenge media (M9 minimal media supplemented with 20 mM D-glucose, 0.5 mM 5-aminolevulinic acid, 0.05 mM IPTG, 0.01% L-arabinose, and NMN^+ as noted). Lpd Ortho (*Ec* Lpd G182R-I186T-M206E-E205W-I271L-R292E-Q317L). Bars represent an average of three biological replicates with error bars of one standard deviation. $NaMN^+$, nicotinic acid mononucleotide; NR, nicotinamide riboside; NMN^+, nicotinamide mononucleotide; NMNH, reduced NMN; AcCoA, acetyl-coenzyme A; *aceE*, pyruvate dehydrogenase; *aceF*, dihydrolipoyllysine-residue acetyltransferase; *lpd*, dihydrolipoyl dehydrogenase; *pflB*, pyruvate-formate lyase; *pncC*, NMN^+ amidohydrolase; *ushA*, 5′-nucleotidase; XenA, xenobiotic reductase A.

In M9 minimal media with 20 mM glucose and 0 mM NMN^+, complementation with Lpd WT restores growth as expected (Figure 3B). When an empty plasmid is supplied, almost no growth is observed, which suggests that the strain's growth is a sensitive readout for completion of the full PDHc catalytic cycle. Supplying Lpd Ortho leads to growth restoration in the media supplemented with 0 mM to 5 mM NMN^+, although growth is rescued slowly in the absence of NMN^+ (Figure S5). To rule out unexpected effects of NMN^+ supplementation on the growth phenotype, we also tested an

https://doi.org/10.1021/acscatal.4c02131
ACS Catal. 2024, 14, 9776−9784

empty plasmid with 0.25 mM NMN^+ supplementation. Again, almost no growth is observed (Figure S6). The cofactor promiscuous enoate reductase (encoded by the gene *Pseudomonas putida xenA*) was also expressed as a redox partner to cycle NMNH generated by Lpd Ortho by reduction of endogenously available substrates[18,36] (e^- acceptors).

The observed NMN^+-dependent growth phenotype for Lpd Ortho indicates that the variant is still capable of fulfilling its role in the context of the full PDHc catalytic cycle. This in vivo readout also highlights the enzyme's orthogonality for NMN^+ in physiological conditions, which cannot be evaluated by kinetic studies in vitro.

CONCLUSIONS

Here, we redesign the coenzyme specificity of the pyruvate dehydrogenase multienzyme complex by systematic mutation of the cofactor binding domain; this converts the enzyme into one displaying specificity for the noncanonical redox cofactor, NMN(H). Through rational design and molecular simulation, we achieve variant Lpd Ortho, which displays marked preference for a model orthogonal redox cofactor at the intracellular concentrations of NAD^+ and $NADP^+$ in *E. coli*.[37] We observe that our remodel of the cofactor binding domain for noncanonical specificity leaves the substrate recognition and the capacity to assemble an active PDHc intact, as determined by the PDHc-coupled growth study. This observation is consistent with the seminal reports of dehydrogenase cofactor specificity engineering by Perham and coworkers on this enzyme class for the native cofactors.[38,39] These results enable the storage of insulated reducing equivalents from the high flux and nearly irreversible reaction of PDHc for direct supply to orthogonal metabolic pathways. Alternatively, Lpd is incorporated into multiple complexes with unique roles in central metabolism beyond that of PDHc. Future work could explore Lpd Ortho's utility in growth coupling since it is incorporated into 2-ketoglutarate dehydrogenase and the glycine cleavage system as well.

Remarkably, extensive rational design initially failed to eliminate Lpd Penta's NAD^+-dependent activity. We propose that the natural cofactor is no longer held in the canonical binding pocket conserved in Rossmann fold dehydrogenases, as the enzyme's cofactor binding site is substantially remodeled. Computational simulations identified alternative cofactor binding sites that are unintuitive to predict; disrupting modeled NAD^+ contacts at these sites were critical to creating Lpd Ortho. This emphasizes a previously overlooked layer in the methodology of developing orthogonal cofactor-specific enzymes: while in the established art of switching cofactor specificity between NAD(H) and NADP(H), the cofactor's position is treated as relatively fixed, cofactor pose migration to alternative sites should also be considered when switching cofactor specificity between natural and noncanonical cofactors.

Remodeling enzymes to specifically interface with bio-orthogonal reagents presents unique challenges in protein engineering. Tailoring enzymes toward noncanonical cofactor specificity requires overcoming two distinct hurdles: discovery of variants that elicit improved noncanonical redox activities and prediction of residues that only participate in interactions with the native dinucleotide cofactors. Our work indicates that the active site can extensively deviate from supporting conserved binding modes during this process and produce cofactor binding poses with little similarity to the canonical ones. To block the adventitious dinucleotide activities observed, we employed a Rosetta workflow that assists in specificity tuning by predicting ancillary cofactor binding sites. While rational design coupled with computational prediction affords variants with improved orthogonality, the complexity of optimizing both high noncanonical activity and minimal $NAD(P)^+$ activity warrants future work to establish high throughput strategies for directed evolution. We envision growth selection, and microfluidics-based platforms will greatly accelerate this effort.[16,22,27,29,40] This future work will expand access to enzymes capable of specific electron delivery and will close the gap in catalytic efficiency between Nature's biocatalysts and our first generation of orthogonal biocatalysts.

This work also adds to the NMN(H)-dependent enzyme toolbox that we and others have been developing.[41] Compared to other enzymes that reduce NMN^+ using glucose, phosphite, or intermediates of glycolysis or the pentose phosphate pathway as the substrates, the k_{cat} of the engineered Lpd reported here is relatively high, which is consistent with its demonstrated activity *in vivo* to sustain cell growth.

METHODS

Media, Buffers, and Cultivation. Routine culture was performed with 2x YT media with antibiotics at concentrations of 100 mg/L ampicillin, 50 mg/L spectinomycin, 50 mg/L kanamycin, or 10 mg/L tetracycline as appropriate. 2x YT contained 16 g/L tryptone, 10 g/L yeast extract, and 5 g/L NaCl. M9 wash buffer consisted of 1 mM $MgSO_4$, 0.1 mM $CaCl_2$, and BD Difco M9 salts (Na_2HPO_4 6.78 g/L, KH_2PO_4 3g/L, NaCl 0.5 g/L, and NH_4Cl 1 g/L). M9 growth challenge media is M9 wash buffer with an additional 20 mM D-glucose, 0.5 mM 5-aminolevulinic acid, 0.05 mM IPTG, 0.01% L-arabinose, and Sigma-Aldrich trace metal mix A5 with Co (H_3BO_3 2860 μg/L, $MnCl_2 \cdot 4H_2O$ 1810 μg/L, $ZnSO_4$ $7H_2O$ 222 μg/L, Na_2MoO_4, $2H_2O$ 390 μg/L, $CuSO_4$, $5H_2O$ 79 μg/L, $Co(NO_3)_2 \cdot 6H_2O$ 49 μg/L). His-binding buffer contained 50 mM sodium phosphate, pH 7.7, 10 mM imidazole, 300 mM NaCl, and 0.03% Triton X-100. His-wash buffer contained 50 mM sodium phosphate pH 7.7, 50 mM imidazole, 300 mM NaCl, and 0.03% Triton X-100. His-elution buffer contained 50 mM sodium phosphate, pH 7.7, 250 mM imidazole, and 300 mM NaCl.

Plasmid and Strain Construction. All plasmids and strains used in this study are summarized in Table S1. Plasmid construction was conducted by Gibson isothermal assembly.[42] Site-directed mutagenesis was performed by PCR with the KOD One Blue DNA polymerase (Toyobo) and primers containing the desired substitutions. Plasmid amplification was performed with *E. coli* XLI-Blue (Stratagene). Plasmid purification was conducted using the QIAprep Spin Miniprep Kit (Qiagen), and sequences were confirmed by Sanger Sequencing (Laragen).

E. coli lpd gene was amplified by PCR from the genome of *E. coli* BW25113 with 25 nucleotides of homology to the pQE vector backbone (N-terminal 6× His-tag, ColE1 *ori*, and Amp^R), purified by agarose gel electrophoresis, and ligated by Gibson assembly to construct pEK14. Plasmids encoding mutants were built through site-directed mutagenesis on the pEK14 template.

E. coli strain MX701 (Δ*lpd* Δ*pncC* R^0) was constructed from the JW0112 (Δ*lpd*::kan) strain of the Keio collection[43] by P1 transduction[44] from strain JW2670−1 (Δ*pncC*::kan) followed by removal of the kanamycin resistance gene by plasmid

https://doi.org/10.1021/acscatal.4c02131
ACS Catal. 2024, 14, 9776−9784

pCP20.[45] Gene deletion was confirmed by colony PCR using a MyTaq HS Red Mix (Bioline). 2x YT media supplemented with 0.5 g/L sodium acetate was used to routinely culture strains with the *lpd* disrupted. *E. coli* strain SW7 (Δ*lpd* Δ*pncC* Δ*ushA*::tet) was constructed from MX701 using the recombination method described by Datsenko and Wanner.[46] Linear donor fragments encoding the tetracycline resistance gene (*tet*) flanked by FRT sites were generated by PCR. Approximately 500 nucleotides of homology on each side were introduced by splicing-by-overlap extension PCR using the KOD Hot Start Xtreme DNA polymerase (Novagen).

E. coli strain SW3 (Δ*lpd* Δ*pncC* Δ*ushA*::tet Δ*pflB*) was prepared from the strain SW7 by CRISPR-Cas9 system,[47] and 0.5 g/L sodium acetate and tetracycline were supplemented to all media. Both editing plasmids were cured prior to growth studies by addition of 1 mM IPTG followed by culture at 37 °C for removal of pTargetF and pCas, respectively.

Protein Expression and Purification. Protein was expressed with an N-terminal 6× His-tag from the pQE vector for immobilized metal affinity chromatography. *E. coli* Δ*lpd*::kan chemical competent cells were prepared following the manufacturer's instructions for the Mix & Go! *E. coli* Transformation Kit (Zymo). Strain Δ*lpd*::kan was transformed with plasmids bearing *lpd* variants and deposited on 2x YT agar plates containing 100 mg/L ampicillin and 0.5 g/L sodium acetate. A single colony was used to inoculate seed cultures in 4 mL 2x YT-200 mg/L ampicillin-0.5 g/L sodium acetate and grown with agitation for 15 h at 37 °C, 250 rpm. 20 mL of the same media was inoculated to 0.07 OD_{600} in a 50 mL conical tube with loose cap. After 1 h and 45 min of growth at 37 °C, the cultures were removed from the incubator. Protein expression was induced by addition of 0.5 mM IPTG, and the culture was grown for additional 18−24 h at 30 °C.

Cells were pelleted at 2500 *g* for 20 min at 4 °C. Cell pellets were lysed by bead-beating with 0.1 mm diameter glass beads in cold His-binding buffer containing 0.15 mM FAD. Protein purification was performed using HisPur Ni NTA resin (Thermo Scientific) according to the manufacturer's instructions using the buffers described above. Protein was quantified by a Bradford assay relative to a BSA standard curve and stored with 20% glycerol at −80 °C until use.

Lpd Activity Assay. Specific activity assay was initiated by the addition of purified enzyme to the assay master mix. Assay condition was 3 mM DL-lipoic acid reduced (Sigma-Aldrich) prepared as a 300 mM stock in ethanol, 100 mM potassium phosphate pH 8.0, 1.5 mM ethylenediaminetetraacetic acid (EDTA), and 6 mM cofactor at 37 °C. The reaction rate was followed by change in absorbance at 340 nm on a SpectraMax plate reader with SoftMax Pro 7.0 software. Final activities were corrected by a no-substrate control.

Determination of Michaelis−Menten kinetic parameters was conducted under the same conditions at eight concentrations of cofactor. Initial reaction rates corrected by a no-substrate control were fit to the Michaelis−Menten equation.

NMN^+-Dependent Growth Study. The NMN^+-dependent growth study was performed as follows. Strain SW3 cells were transformed with plasmids carrying genes encoding the Lpd variants or controls along with a plasmid encoding XenA D116E by electroporation, followed by an outgrowth of 1.5 h at 37 °C in 2x YT with 0.5 g/L sodium acetate. Transformants were deposited on plates, and single colonies were used to inoculate seed cultures of 4 mL 2x YT with ampicillin, spectinomycin, and sodium acetate. After 15−18 h at 37 °C, cells were washed three times in 1 mL M9 wash buffer and then resuspended to a final concentration of 1.0 OD_{600} in M9 wash buffer. The growth study was initiated by the addition of washed cells to 1 mL of M9 growth challenge media described above with either 0 or 0.25 mM NMN^+ at a starting OD_{600} of 0.01. Cells were cultured for growth study in 2 mL square 96-well plate with V-bottom shaking on a 3 mm orbit at 800 rpm.

Modeling of Cofactor−Enzyme Interactions. The FAD-bound crystal structure of Lpd (PDB: 4JDR) served as the template for the ligand docking simulations.[48] For the initial placement of NAD^+ in the crystal structure, AlphaFill was used.[49] The refinement of protein−ligand interactions utilized Rosetta's backbone constrained FastRelax protocol.[50] Mutant structures were modeled by applying the mutations to the energy-minimized structure using the MutateResidue Rosetta mover,[51] prior to any optimization of the cofactor-enzyme complex.

Conformer libraries for NMN^+, NAD^+, and $NADP^+$ were prepared according to previous research.[18,19] We hypothesized that the catalytically relevant position of the nicotinamide moiety of NMN^+ and $NADP^+$ would be similar to that of NAD^+. Therefore, for all docking simulations, the initial placements of the cofactors in the active site were based on the coordinates of the nicotinamide ring and carboxamide group from the energy-minimized AlphaFill model. 2000 simulations were conducted, where distance and angle constraints were enforced during energy minimization to maintain the cofactors in catalytically competent geometry for hydride transfer in relation to FAD.

For investigating alternative binding modes, PredesignPerturbMover was used to randomly move the cofactor within the active site. This mover temporarily transforms the surrounding residues into alanines, potentially avoiding steric barriers imposed by constraining the backbone atoms. For investigating mutational effects, the transform mover was used to perform a Monte Carlo search of the ligand binding site without the temporary alanine transformation.

For each batch's analysis, the top 20 scoring outputs were selected based on constraint score, protein−ligand interface energy score, and total system energy score. The Supporting Information contains a GitHub link with example run files, including constraints, options, RosettaScripts XML, and ligand params.

■ ASSOCIATED CONTENT

Supporting Information

The Supporting Information is available free of charge at https://pubs.acs.org/doi/10.1021/acscatal.4c02131.

Extended methods; plasmids and strains used in this study; specific activity of Lpd WT, Lpd Double, and Lpd Triple; structural alignment of *Lp* Nox and *Ec* Lpd; specific activity of Lpd RA4 (Lpd Penta); analysis of M206 reversion variant; growth of SW3 with varying NMN^+ concentrations; growth of SW3 bearing an empty plasmid with NMN^+ supplementation; and Rosetta example run files (PDF)

■ AUTHOR INFORMATION

Corresponding Author

Han Li − *Department of Chemical and Biomolecular Engineering, University of California, Irvine, Irvine, California 92697-3900, United States; Department of*

https://doi.org/10.1021/acscatal.4c02131
ACS Catal. 2024, 14, 9776−9784

Biomedical Engineering and Department of Biological Chemistry, University of California, Irvine, Irvine, California 92697-3900, United States; orcid.org/0000-0002-6113-6433; Email: han.li@uci.edu

Authors

Derek Aspacio − *Department of Chemical and Biomolecular Engineering, University of California, Irvine, Irvine, California 92697-3900, United States*

Emma Luu − *Genome Center, University of California, Davis, Davis, California 95616, United States*

Suphanida Worakaensai − *Department of Chemical and Biomolecular Engineering, University of California, Irvine, Irvine, California 92697-3900, United States*

Youtian Cui − *Genome Center, University of California, Davis, Davis, California 95616, United States;* orcid.org/0000-0002-7138-2566

Sarah Maxel − *Department of Chemical and Biomolecular Engineering, University of California, Irvine, Irvine, California 92697-3900, United States*

Edward King − *Department of Molecular Biology and Biochemistry, University of California, Irvine, Irvine, California 92697-3900, United States*

Raine Hagerty − *Department of Biomedical Engineering, University of California, Irvine, Irvine, California 92697-3900, United States*

Alexander Chu − *Department of Chemical and Biomolecular Engineering, University of California, Irvine, Irvine, California 92697-3900, United States*

Derek Minn − *Department of Chemical and Biomolecular Engineering, University of California, Irvine, Irvine, California 92697-3900, United States*

Justin B. Siegel − *Genome Center, University of California, Davis, Davis, California 95616, United States; Department of Chemistry and Department of Biochemistry and Molecular Medicine, University of California, Davis, Davis, California 95616, United States*

Complete contact information is available at: https://pubs.acs.org/10.1021/acscatal.4c02131

Author Contributions

#D.A., E.L., and S.W. contributed equally. D.A., S.W., S.M., E.K., and H.L. designed the experiments. E.L. and Y.C. performed Rosetta modeling and prediction. S.W., D.A., E.K., S.M., R.H., A.C., and D.M. performed the rational protein engineering experiments. S.W. and D.A. performed the apparent Michaelis−Menten kinetic experiments. S.W., S.M., and D.A. performed the strain construction. D.A. and S.W. performed the PDHc growth restoration studies. E.L., Y.C., and J.S. analyzed the modeling results. All authors analyzed the data and wrote the manuscript.

Notes

The authors declare no competing financial interest.

ACKNOWLEDGMENTS

H.L. acknowledges support from University of California, Irvine, the National Science Foundation (NSF) (award no. 1847705), and the National Institutes of Health (NIH) (award no. DP2 GM137427), Alfred Sloan Research Fellowship, and Advanced Research Projects Agency−Energy (ARPA-E) (award no. DE-AR0001508). E.L. and J.B.S. acknowledge the support from Advanced Research Projects Agency−Energy (ARPA-E) (award no. DE-AR0001508). Y.C. and J.B.S. acknowledge the funding of the National Institute of Environmental Health Sciences Grant Number: P42ES004699, the National Institutes of Health Grant Number R01 GM 076324-11, and the National Science Foundation Grant Numbers: 1627539, 1805510, 1827246. R.L. acknowledges support from the National Institutes of Health (NIH) (award no. GM130367). D.A. acknowledges support from the NSF Graduate Research Fellowship Program (grant no. DGE1839285). S.M. acknowledges support from the NSF Graduate Research Fellowship Program (grant no. DGE1839285). S.W. acknowledges support from the Development and Promotion of Science and Technology Talents Project (DPST) Scholarship (grant no. 592017-1/59).

REFERENCES

(1) Liu, Y.; et al. Biofuels for a sustainable future. *Cell* **2021**, *184*, 1636−1647.

(2) Liao, J. C.; Mi, L.; Pontrelli, S.; Luo, S. Fuelling the future: Microbial engineering for the production of sustainable biofuels. *Nat. Rev. Microbiol.* **2016**, *14*, 288−304.

(3) Weusthuis, R. A.; Folch, P. L.; Pozo-Rodríguez, A.; Paul, C. E. Applying Non-canonical Redox Cofactors in Fermentation Processes. *iScience* **2020**, *23*, 101471.

(4) Zhang, Y. H. P. Simpler is better: High-yield and potential low-cost biofuels production through cell-free synthetic pathway biotransformation (SyPaB). *ACS Catal.* **2011**, *1*, 998−1009.

(5) Bowie, J. U.; et al. Synthetic Biochemistry: The Bio-inspired Cell-Free Approach to Commodity Chemical Production. *Trends Biotechnol.* **2020**, *38*, 766−778.

(6) Job Zhang, Y.-H. P.; Zhu, Z.; You, C.; Zhang, L.; Liu, K. In Vitro BioTransformation (ivBT): Definitions, Opportunities, and Challenges. *Synth. Biol. Eng.* **2023**, *1*, No. 10013.

(7) Kunjapur, A. M.; Tarasova, Y.; Prather, K. L. J. Synthesis and accumulation of aromatic aldehydes in an engineered strain of escherichia coli. *J. Am. Chem. Soc.* **2014**, *136*, 11644−11654.

(8) Rodriguez, G. M.; Atsumi, S. Toward aldehyde and alkane production by removing aldehyde reductase activity in Escherichia coli. *Metab. Eng.* **2014**, *25*, 227−237.

(9) Pyne, M. E.; et al. A yeast platform for high-level synthesis of tetrahydroisoquinoline alkaloids. *Nat. Commun.* **2020**, *11*, 3337.

(10) Zhang, Y.-H. P.; Sun, J.; Ma, Y. Biomanufacturing: history and perspective. *J. Ind. Microbiol. Biotechnol.* **2017**, *44*, 773−784.

(11) You, C.; et al. An in vitro synthetic biology platform for the industrial biomanufacturing of myo-inositol from starch. *Biotechnol. Bioeng.* **2017**, *114*, 1855−1864.

(12) Campbell, E.; Meredith, M.; Minteer, S. D.; Banta, S. Enzymatic biofuel cells utilizing a biomimetic cofactor. *Chem. Commun.* **2012**, *48*, 1898.

(13) Rollin, J. A.; Tam, T. K.; Zhang, Y.-H. P. New biotechnology paradigm: cell-free biosystems for biomanufacturing. *Green Chem.* **2013**, *15*, 1708.

(14) Huang, R.; Chen, H.; Upp, D. M.; Lewis, J. C.; Zhang, Y. H. P. J. A High-Throughput Method for Directed Evolution of NAD(P)+-Dependent Dehydrogenases for the Reduction of Biomimetic Nicotinamide Analogues. *ACS Catal.* **2019**, *9*, 11709−11719.

(15) Meng, D.; et al. Coenzyme Engineering of Glucose-6-phosphate Dehydrogenase on a Nicotinamide-Based Biomimic and Its Application as a Glucose Biosensor. *ACS Catal.* **2023**, *13*, 1983−1998.

(16) Zachos, I.; et al. Hot Flows: Evolving an Archaeal Glucose Dehydrogenase for Ultrastable Carba-NADP $^{+}$ Using Microfluidics at Elevated Temperatures. *ACS Catal.* **2022**, *12*, 1841−1846.

(17) Zachos, I.; Döring, M.; Tafertshofer, G.; Simon, R. C.; Sieber, V. carba Nicotinamide Adenine Dinucleotide Phosphate: Robust Cofactor for Redox Biocatalysis. *Angew. Chem., Int. Ed.* **2021**, *60*, 14701−14706.

(18) Black, W. B.; et al. Engineering a nicotinamide mononucleotide redox cofactor system for biocatalysis. *Nat. Chem. Biol.* **2020**, *16*, 87−94.
(19) King, E.; et al. Engineering Embden−Meyerhof−Parnas Glycolysis to Generate Noncanonical Reducing Power. *ACS Catal.* **2022**, *12*, 8582−8592.
(20) Richardson, K. N.; Black, W. B.; Li, H. Aldehyde Production in Crude Lysate- and Whole Cell-Based Biotransformation Using a Noncanonical Redox Cofactor System. *ACS Catal.* **2020**, *10*, 8898−8903.
(21) Maxel, S.; et al. A Growth-Based, High-Throughput Selection Platform Enables Remodeling of 4-Hydroxybenzoate Hydroxylase Active Site. *ACS Catal.* **2020**, *10*, 6969−6974.
(22) Aspacio, D.; et al. Shifting Redox Reaction Equilibria on Demand Using an Orthogonal Redox Cofactor. *bioRxiv* **2023**, No. 2023.08.29.555398.
(23) Wang, X.; et al. Creating enzymes and self-sufficient cells for biosynthesis of the non-natural cofactor nicotinamide cytosine dinucleotide. *Nat. Commun.* **2021**, *12*, 2116.
(24) Ji, D.; et al. Creation of Bioorthogonal Redox Systems Depending on Nicotinamide Flucytosine Dinucleotide. *J. Am. Chem. Soc.* **2011**, *133*, 20857−20862.
(25) Guo, X.; et al. Non-natural Cofactor and Formate-Driven Reductive Carboxylation of Pyruvate. *Angew. Chem.* **2020**, *132*, 3167−3170.
(26) Huang, R.; Chen, H.; Upp, D. M.; Lewis, J. C.; Zhang, Y.-H. P. J. A High-Throughput Method for Directed Evolution of NAD(P) + -Dependent Dehydrogenases for the Reduction of Biomimetic Nicotinamide Analogues. *ACS Catal.* **2019**, *9*, 11709−11719.
(27) Zhang, L.; et al. Directed evolution of phosphite dehydrogenase to cycle noncanonical redox cofactors via universal growth selection platform. *Nat. Commun.* **2022**, *13*, 5021.
(28) Black, W. B.; et al. Metabolic engineering of Escherichia coli for optimized biosynthesis of nicotinamide mononucleotide, a non-canonical redox cofactor. *Microb. Cell Fact.* **2020**, *19*, 150.
(29) King, E.; et al. Orthogonal glycolytic pathway enables directed evolution of noncanonical cofactor oxidase. *Nat. Commun.* **2022**, *13*, 7282.
(30) Meiler, J.; Baker, D. ROSETTALIGAND: Protein-small molecule docking with full side-chain flexibility. *Proteins Struct. Funct. Bioinforma.* **2006**, *65*, 538−548.
(31) Noor, E.; Eden, E.; Milo, R.; Alon, U. Central Carbon Metabolism as a Minimal Biochemical Walk between Precursors for Biomass and Energy. *Mol. Cell* **2010**, *39*, 809−820.
(32) Wenk, S.; et al. An "energy-auxotroph" Escherichia coli provides an in vivo platform for assessing NADH regeneration systems. *Biotechnol. Bioeng.* **2020**, *117*, 3422−3434.
(33) Galeazzi, L.; et al. Identification of nicotinamide mononucleotide deamidase of the bacterial pyridine nucleotide cycle reveals a novel broadly conserved amidohydrolase family. *J. Biol. Chem.* **2011**, *286*, 40365−40375.
(34) Kakehi, M.; Usuda, Y.; Tabira, Y.; Sugimoto, S. Complete deficiency of 5′-nucleotidase activity in Escherichia coli leads to loss of growth on purine nucleotides but not of their excretion. *J. Mol. Microbiol. Biotechnol.* **2007**, *13*, 96−104.
(35) Wang, L.; et al. Identification of UshA as a major enzyme for NAD degradation in Escherichia coli. *Enzyme Microb. Technol.* **2014**, *58*−*59*, 75−79.
(36) Stott, K.; Saito, K.; Thiele, D. J.; Massey, V. Old Yellow Enzyme. The discovery of multiple isozymes and a family of related proteins. *J. Biol. Chem.* **1993**, *268*, 6097−6106.
(37) Bennett, B. D. et al. Site Occupancy in Escherichia coli, 2010, *5*, 593−599.
(38) Bocanegra, J. A.; Scrutton, N. S.; Perham, R. N. Creation of an NADP-dependent pyruvate dehydrogenase multienzyme complex by protein engineering. *Biochemistry* **1993**, *32*, 2737−2740.
(39) Nigel, S.; Berry, A.; Perham, R. Redesign of the coenzyme specificity of a dehygrogenase by protein engineering. *Nature* **1990**, *343*, 38−43.
(40) King, E.; Maxel, S.; Li, H. Engineering natural and noncanonical nicotinamide cofactor-dependent enzymes: design principles and technology development. *Curr. Opin. Biotechnol.* **2020**, *66*, 217−226.
(41) Black, W. B.; Perea, S.; Li, H. Design, construction, and application of noncanonical redox cofactor infrastructures. *Curr. Opin. Biotechnol.* **2023**, *84*, 103019.
(42) Gibson, D. G.; et al. Enzymatic assembly of DNA molecules up to several hundred kilobases. *Nat. Methods* **2009**, *6*, 343−345.
(43) Baba, T.; et al. Construction of Escherichia coli K-12 in-frame, single-gene knockout mutants: The Keio collection. *Mol. Syst. Biol.* **2006**, *2*, 2006.0008.
(44) Thomason, L. C.; Costantino, N.; Court, D. L. E. coli Genome Manipulation by P1 Transduction. *Curr. Protoc. Mol. Biol.* **2007**, 1.17.1−1.17.8.
(45) Cherepanov, P. P.; Wackernagel, W. Gene disruption in Escherichia coli: TcR and KmR cassettes with the option of Flp-catalyzed excision of the antibiotic-resistance determinant. *Gene* **1995**, *158*, 9−14.
(46) Datsenko, K. A.; Wanner, B. L. One-step inactivation of chromosomal genes in *Escherichia coli* K-12 using PCR products. *Proc. Natl. Acad. Sci. U. S. A.* **2000**, *97*, 6640−6645.
(47) Jiang, Y.; et al. Multigene editing in the Escherichia coli genome via the CRISPR-Cas9 system. *Appl. Environ. Microbiol.* **2015**, *81*, 2506−2514.
(48) Chandrasekhar, K.; et al. Insight to the Interaction of the Dihydrolipoamide Acetyltransferase (E2) Core with the Peripheral Components in the Escherichia coli Pyruvate Dehydrogenase Complex via Multifaceted Structural Approaches. *J. Biol. Chem.* **2013**, *288*, 15402−15417.
(49) Hekkelman, M. L.; de Vries, I.; Joosten, R. P.; Perrakis, A. AlphaFill: enriching AlphaFold models with ligands and cofactors. *Nat. Methods* **2023**, *20*, 205−213.
(50) Tyka, M. D.; et al. Alternate States of Proteins Revealed by Detailed Energy Landscape Mapping. *J. Mol. Biol.* **2011**, *405*, 607−618.
(51) Fleishman, S. J.; et al. RosettaScripts: A Scripting Language Interface to the Rosetta Macromolecular Modeling Suite. *PLoS One* **2011**, *6*, No. e20161.

https://doi.org/10.1021/acscatal.4c02131
ACS Catal. 2024, 14, 9776−9784